Supporting Information:

Computational mining of photocatalysts for water splitting hydrogen production: two dimensional InSe-family monolayers

Qiong Peng[1], Rui Xiong[1], Baisheng Sa[1,2,*], Jian Zhou[2], Cuilian Wen[1], Bo Wu[1,**], Masakazu Anpo[3] and Zhimei Sun[2,***]

[1]*Multiscale Computational Materials Facility, College of Materials Science and Engineering, Fuzhou University, and Key Laboratory of Eco-materials Advanced Technology (Fuzhou University), Fujian Province University, Fuzhou 350100, P. R. China*

[2]*School of Materials Science and Engineering, and Center for Integrated Computational Materials Engineering, International Research Institute for Multidisciplinary Science, Beihang University, Beijing 100191, P. R. China*

[3]*Department of Applied Chemistry, Graduate School of Engineering, Osaka Prefecture University, Sakai, Osaka, Japan*

Corresponding Authors

B. Sa* E-mail: bssa@fzu.edu.cn

B. Wu** E-mail: wubo@fzu.edu.cn

Z. Sun*** E-mail: zmsun@buaa.edu.cn

In the bulk phase of group-III monochalcogenides, the interlayers are bonded together by weak vdW interactions.[1] It is reported that the HSE+vdW framework can give a very good estimation of structural parameters and electronic structures for the vdW bulk phases over standard DFT functionals.[2,3] To test the best functional combination for the following calculations of monolayer structures, we relaxed the geometry with different vdW functionals and then calculated the band structure by the corresponding HSE+vdW functional for the bulk InSe. As summarized in **Table S1**, the calculated equilibrium lattice constants for bulk InSe are in the range of 3.952~4.097 Å using PBE, optB88-vdW, optB86-vdW, PBE-D2 and PBE-D3 functionals; the difference is less than 0.09 Å compared to the experimental data.[4,5] It is seen from the band structures in **Figure S1** that the bulk InSe is a direct band-gap semiconductor. Compared to the experimental data,[6] the optPBE-vdW and

revPBE-vdW give unexpected large lattice constants and small band gap; and the PBE and PBE-D2 provide a considerably large band gap. From the perspective of structural parameters and band gaps (**Table S1**), the optB86-vdW functional produces fairly good results for the bulk InSe as compared to the experimental data.[4-6] Thus, the optB86-vdW functional could be the best functional combination and employed in the following calculations for monolayer structures.

The initial screening of the MX monolayers as potential photocatalysts is mainly based on their electronic structures and band gaps, which are illustrated in **Figure S5**. The results indicate that the MX monolayers are indirect band gap semiconductors with the band gaps from 1.98 to 3.34 eV. Take the band structure of InSe monolayer as an example, as shown in **Figure S5b** and the inset wave-functions, the CBM locates at the Γ point and is contributed by the hybridization of the In *s* and Se *p* electrons, where the VBM locates between the Γ-K point and is occupied by the hybridization of the In *p* and Se *p* electrons. Since the Se atoms are placed on the outer layer of the 2D material, high activities of holes and electrons on the surface are anticipated. Except for the GaTe monolayer, both the CBM and VBM of the InS, InTe, GaS and GaSe monolayers show very similar characterizations to the InSe monolayer. The VBM of the GaTe monolayer follows InSe as well, but due to the strong hybridization of the Ga *s* electrons and Te *p* electrons (see the inset in **Figure S5f**), the CBM of GaTe is located at the M point. It is worth noting that, for InSe monolayer, the energy level of VBM is only 0.048 eV higher than the valence band states at the Γ point. On the other hand, the energy difference between the actual VBM and the VBM at the Γ point is less than 0.1 eV for all the MX monolayers. More importantly, all MX monolayers exhibit larger band gap than 1.23 eV for photocatalytic water splitting. Herein, the band gaps of the InSe, InTe and GaTe monolayers are 2.18, 1.91 and 2.08 eV, respectively. The favorable band gaps indicating that the InSe, InTe and GaTe

monolayers show ideal electronic structures for the potential photocatalysis applications. And for the InS, GaS and GaSe monolayers, the predicted band gaps of 2.52, 3.27 and 2.71 eV are slightly higher than the expected, which can be tuned by doping[7] or strain engineering[8] to meet the particular requirement of the photocatalysis applications.

Another criterion to facilitate the water splitting hydrogen production reactions is that the CBM is higher than the hydrogen reduction potential (H^+/H_2) and the VBM is lower than the water oxidation potential (H_2O/O_2).[9,10] The calculated band alignments of the six MX monolayers are shown together with the redox potentials of water splitting in **Figure S6**. Here, we estimated the ionization potential for each MX monolayer using a slab model, in which the vacuum level was used as a reference. The energy difference between the vacuum level and the highest occupied molecular orbitals (HOMO) is the minimum energy necessary to remove an electron from the system, and is known as the ionization potential, defined here as a negative quantity.[11] Its equivalent in an organic semiconductor is VBM.[12] In present study, we found that the ionization potential of each MX monolayer situates below the H_2O/O_2 oxidation potential, which is consistent with Zhuang' calculated results.[9] Moreover, the band edges straddle the water redox potentials, contributing to the hydrogen reduction,[13] The results imply that the MX monolayers have great potential for the water oxidation and hydrogen reduction process.

For MX monolayers, we have found some common rules: (i) as the atomic number of X increases (from S to Se to Te), the band gap decreases and VBM energy level increases. Meanwhile, with the increase of the atomic number of X, the CBM energy of InX increases, but the CBM energies of GaX systems are stable around 3.6 eV. (ii) The CBM and VBM energies of GaX are higher than those of InX. These observations agree with previous results using different methods.

Therefore, InS has the lowest CBM and VBM, GaTe has the highest VBM, and GaS has the highest CBM. These results reveal that the n-type doping in InS is easier, but p-type doping in GaS is preferred.

Table S1. Lattice constant a (Å) and HSE06 band gap E_g (eV) of bulk InSe using PBE and different vdW functionals.

System	Method	a	E_g
bulk InSe	PBE	4.097	1.56
	optB88	4.089	0.95
	optB86	4.053	1.08
	PBE-D2	3.952	1.52
	PBE-D3	4.040	1.14
	optPBE	4.116	0.94
	revPBE	4.180	0.83
	Expt.[4-6]	4.05, 4.01	1.17

Table S2. Lattice constant a (Å), M-X and M-M bond length L (Å) of InSe-family MX monolayers.

System	Method	a	L_{M-X}	L_{M-M}
InS	OptB86	3.928	2.568	2.814
InSe	OptB86	4.041	2.689	2.812
	PBE[9,14]	4.09	-	-
	PBE-D2[15]	3.95	-	-
InTe	OptB86	4.364	2.889	2.806
GaS	OptB86	3.646	2.370	2.472
	DFT-D2[1]	3.635	2.368	2.479
GaSe	OptB86	3.813	2.499	2.469
	DFT-D2[1]	3.815	2.5	2.474
GaTe	OptB88	4.126	2.708	2.468
	PBE[16]	4.06	-	-

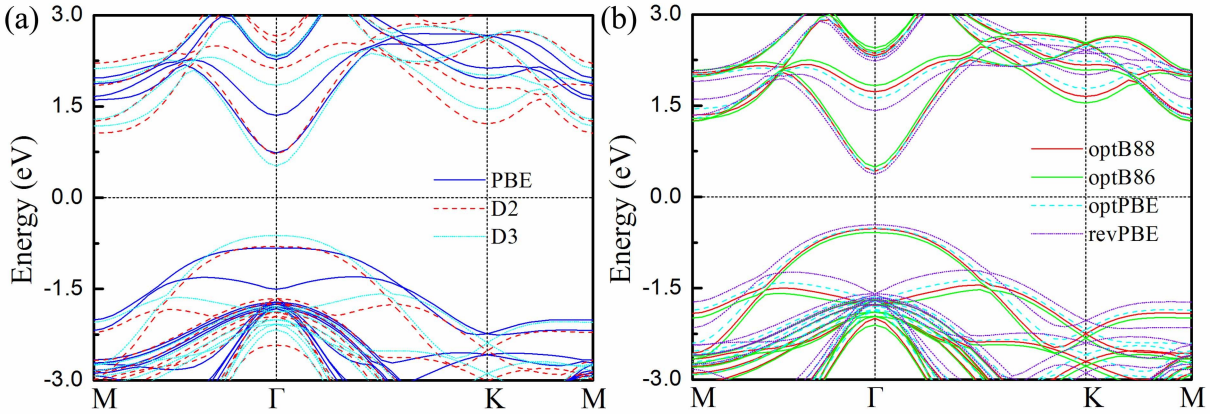

Figure S1. HSE06 band structures of bulk InSe using PBE and different vdW functionals.

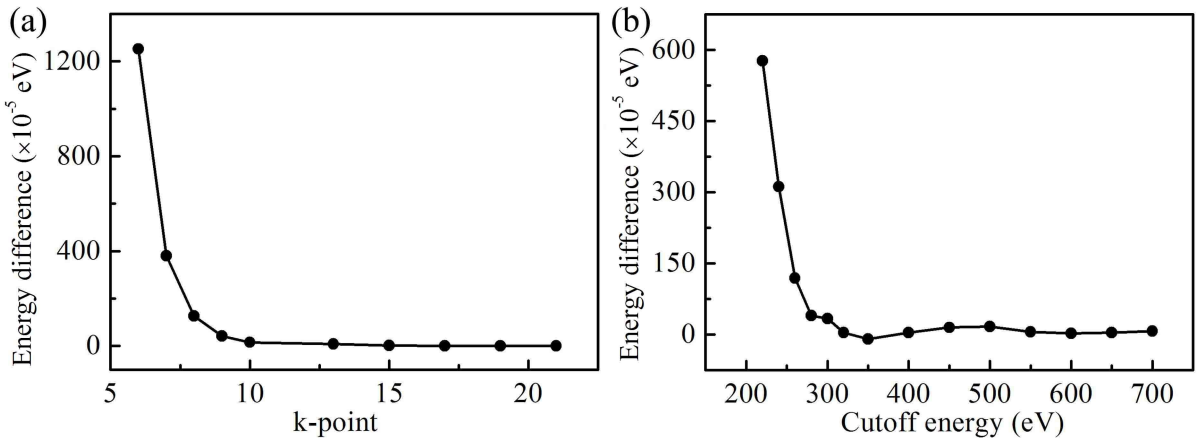

Figure S2. Total energy convergence tests based on different k-point mesh (a) and cutoff energy (b).

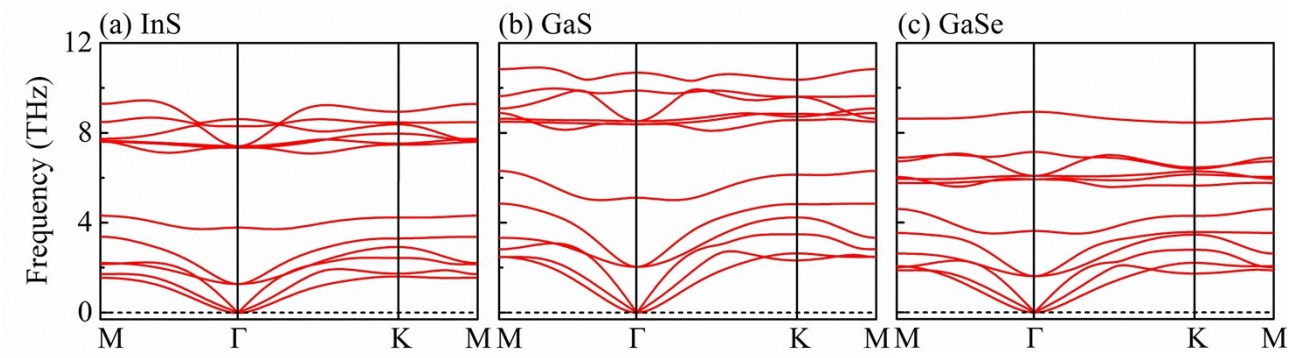

Figure S3. Phonon dispersion curves of (a) InS, (b) GaS and (c) GaSe monolayers.

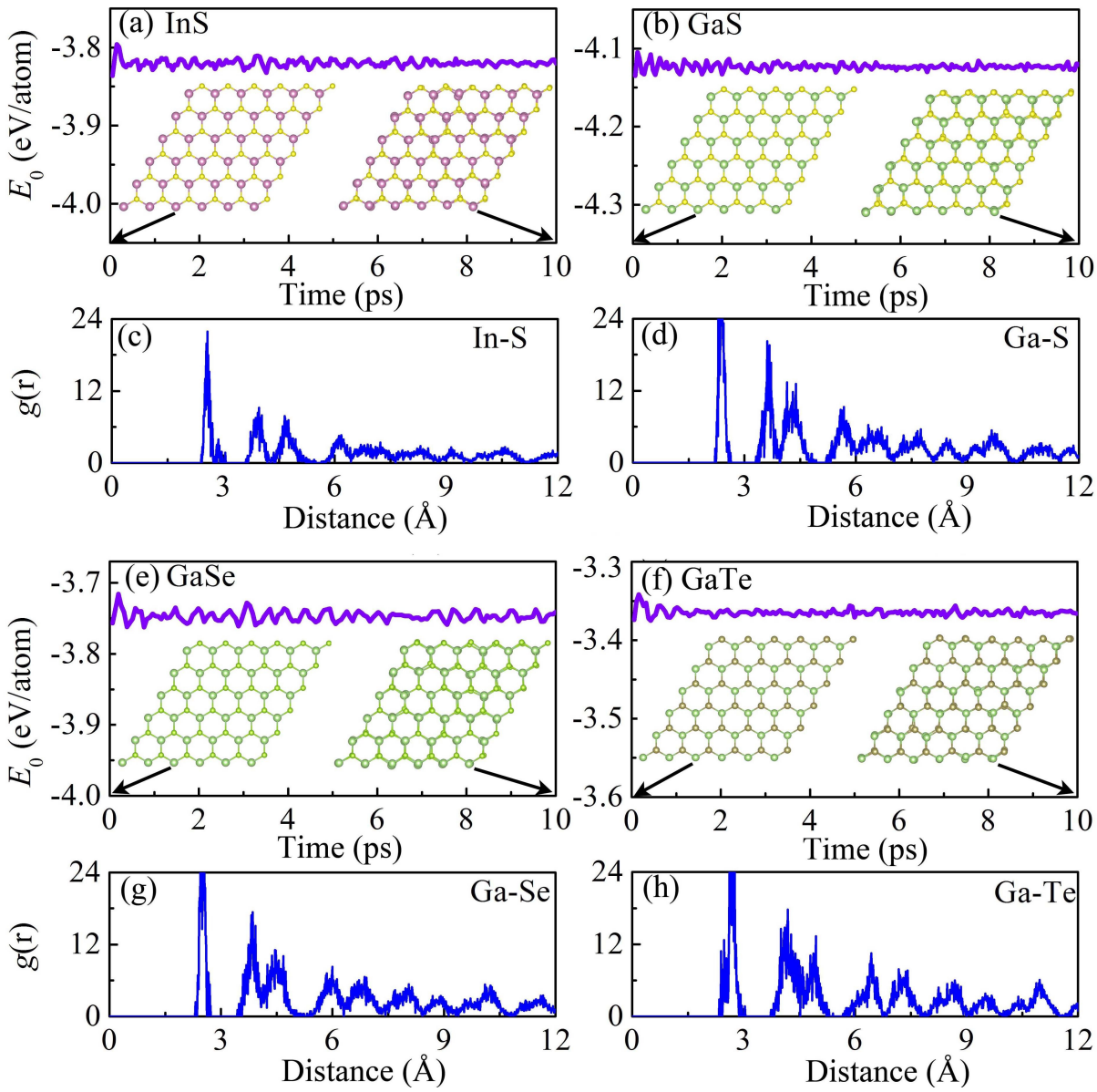

Figure S4. Evolution of total energy of the systems in AIMD and snapshot structures of (a) InS, (b) GaS, (e) GaSe and (f) GaTe monolayers at 0 ps and 10 ps. (c, d, g, h) The normalized pair correlation function g(r) after stabilizing at 300 K for 10 ps.

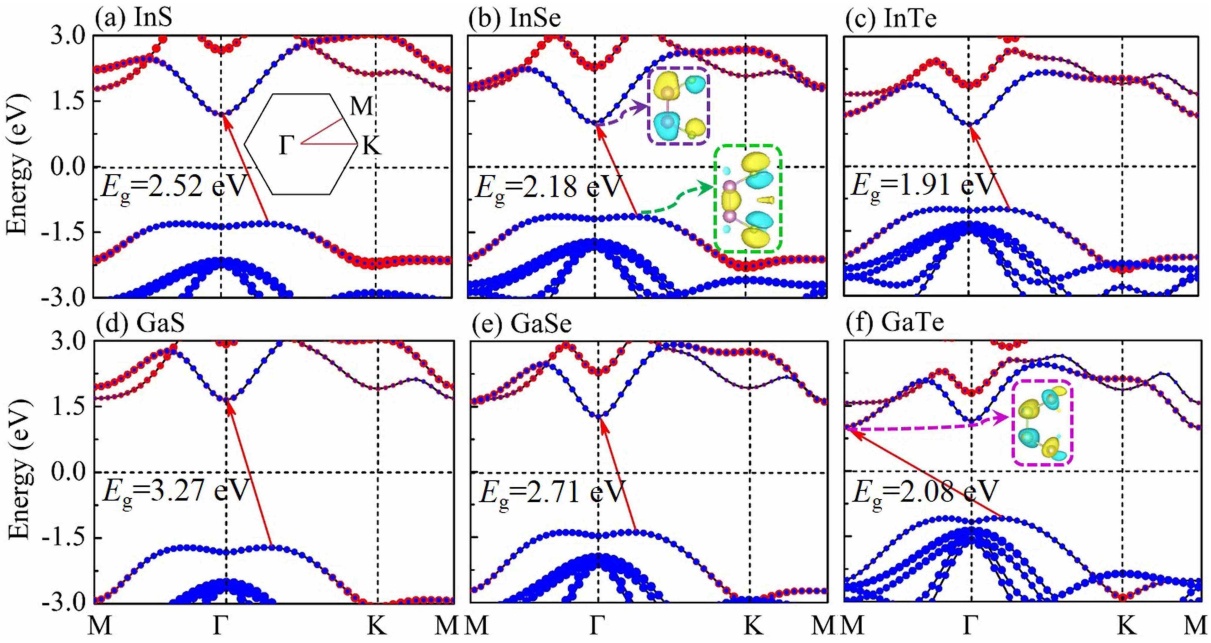

Figure S5. HSE06 projected band structures of (a) InS, (b) InSe, (c) InTe, (d) GaS, (e) GaSe and (f) GaTe monolayers. The Fermi level is set to zero. The size of red and blue dots illustrates the projected weight of M and X atoms, respectively. The contributions of electrons in VBM and CBM are shown in the inset.

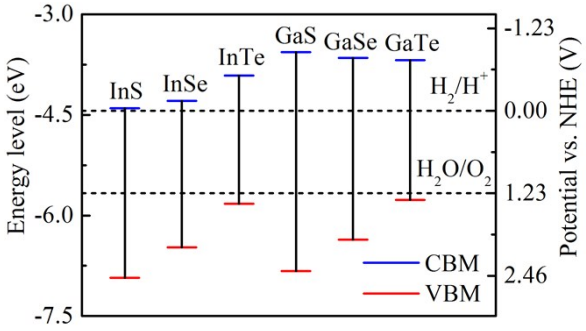

Figure S6. HSE06 band alignments of the MX monolayers. The ionization potential with respect to the vacuum level is represented by the vertical axis and its equivalent is VBM. The black dashed lines indicate the hydrogen reduction potential (H^+/H_2) and water oxidation potential (H_2O/O_2).

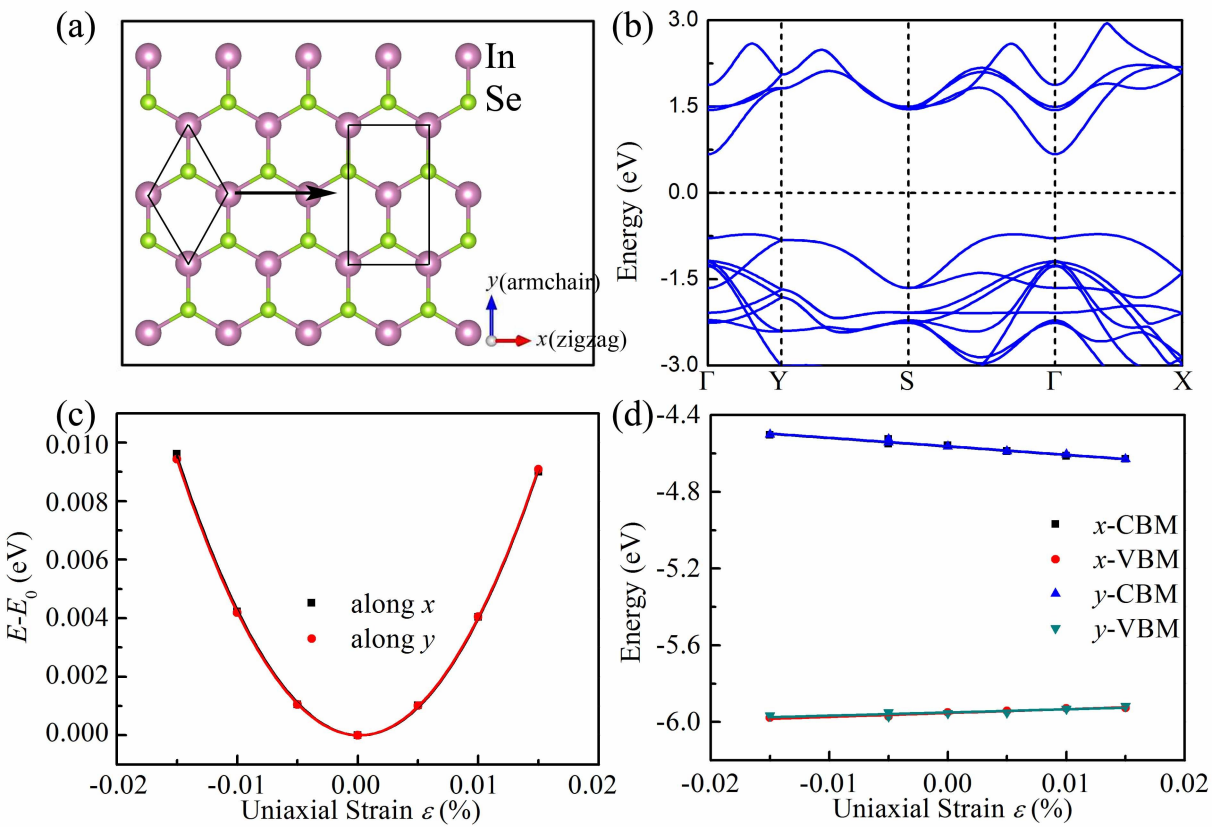

Figure S7. (a) An orthorhombic lattice instead of the traditional hexagonal lattice was adopted to calculate the intrinsic responses to uniaxial strain in single-layer InSe. (b) Band structure of single-layer InSe by PBE. (c) Total energy shift E-E_0 and (d) band edge positions of single-layer InSe as a function of the uniaxial strain ε along the x and y directions by PBE. In (d), the vacuum level is set at zero for reference.

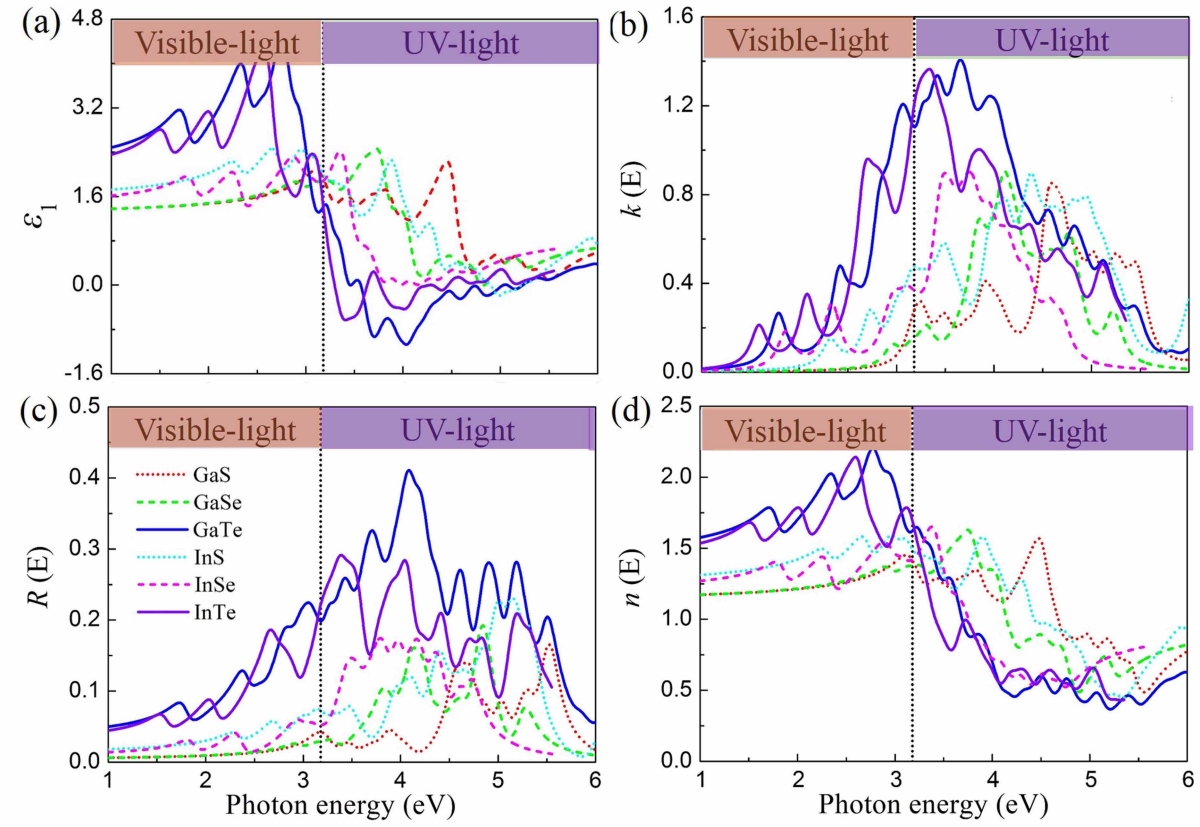

Figure S8. (a) The real part ε_1 of the dielectric function, (b) extinction coefficient *k*, (c) reflectivity coefficient *R*, and (d) optical refractive index *n*.

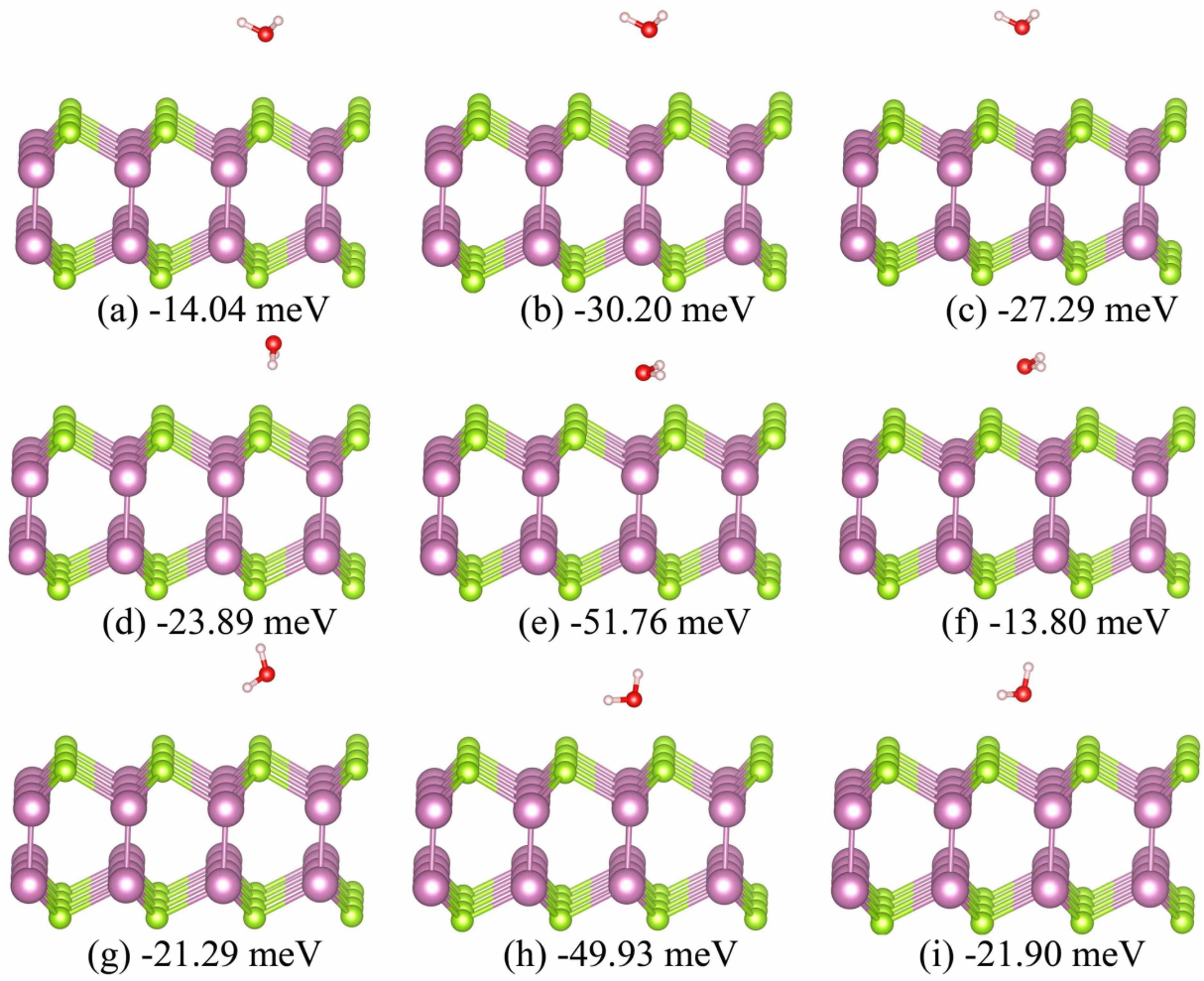

Figure S9. Optimized structures of water molecule on the InSe surface. The computed adsorption energies are shown under the corresponding structures. Coloring scheme: brown (In), green (Se), red (O from water) and magenta (H from water).

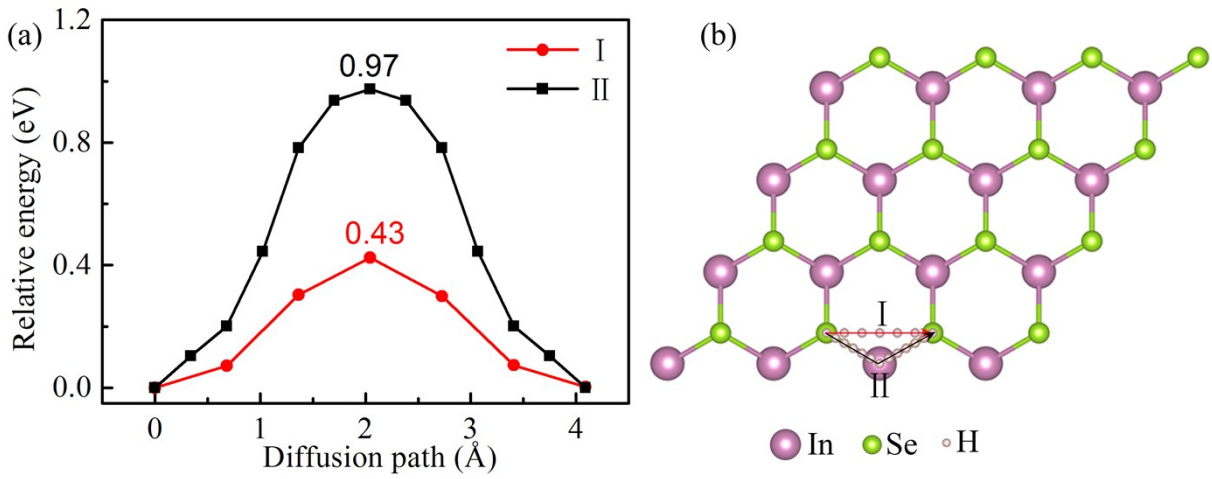

Figure S10. Considered migration paths and the corresponding diffusion energy barrier profiles for one H atom adsorbed on the 2D InSe surface.

References

1 W. Wei, Y. Dai, C. Niu, X. Li, Y. Ma and B. Huang, *J. Mater. Chem. C*, 2015, **3**, 11548-11554.

2 W. Gao and A. Tkatchenko, *Phys. Rev. Lett.*, 2013, **111**, 045501.

3 J. Wang, D. Hao, J. Ye and N. Umezawa, *Chem. Mater.*, 2017, DOI: 10.1021/acs.chemmater.6b02969.

4 S. A. Semiletov, *Kristallografiya*, 1958, **3**, 288-292.

5 B. Čelustka and S. Popović, *J. Phys. Chem. Solids*, 1974, **35**, 287-289.

6 O. Madelung, *Semiconductors: Data Handbook*. Springer Berlin Heidelberg: 2004; p 397-403.

7 Y. Li, Y.-L. Li, C. M. Araujo, W. Luo and R. Ahuja, *Catal.Sci.technol.*, 2013, **3**, 2214-2220.

8 Z. Guo, N. Miao, J. Zhou, B. Sa and Z. Sun, *J. Mater. Chem. C*, 2016, **5**, 978-984.

9 H. L. Zhuang and R. G. Hennig, *Chem. Mater.*, 2013, **25**, 3232-3238.

10 A. K. Singh, K. Mathew, H. L. Zhuang and R. G. Hennig, *J. Phys. Chem. Lett.*, 2015, **6**, 1087-1098.

11 J. Wang, N. Umezawa and H. Hosono, *Adv. Energy Mater.*, 2015, **6**, 1501190.

12 A. Kahn, *Materials Horizons*, 2015, **3**, 7-10.

13 K. Chang, M. Li, T. Wang, S. Ouyang, P. Li, L. Liu and J. Ye, *Adv. Energy Mater.*, 2015, **5**, 1402279.

14 W. Li and J. Li, *Nano Res.*, 2015, **8**, 3796-3802.

15 L. Debbichi, O. Eriksson and S. Lebègue, *J. Phys. Chem. Lett.*, 2015, **6**, 3098-3103.

16 Z. Ni, E. Minamitani, Y. Ando and S. Watanabe, *Phys. Chem. Chem. Phys.*, 2015, **17**, 19039-19044.